

Frictional characteristics of Fusion Deposition Modeling (FDM) manufactured surfaces

Foad Sojoodi Farimani

Department of Biomechanical Engineering, Faculty of Engineering Technology, University of Twente, Enschede, The Netherlands

Matthijn de Rooij

Department of Mechanics of Solids, Surfaces and Systems, University of Twente, Enschede, The Netherlands

Edsko Hekman

Department of Biomechanical Engineering, Faculty of Engineering Technology, University of Twente, Enschede, The Netherlands, and

Sarthak Misra

Department of Biomechanical Engineering, University of Twente, The Netherlands and Department of Biomedical Engineering, University Medical Center Groningen and University of Groningen, The Netherlands

Abstract

Purpose – Additive manufacturing (AM) is a promising alternative to the conventional production methods (i.e., machining), providing the developers with great geometrical and topological freedom during the design and immediate prototyping customizability. However, frictional characteristics of the AM surfaces are yet to be fully explored, making the control and manufacturing of precise assembly manufactured mechanisms (i.e., robots) challenging. The purpose of this paper is to understand the tribological behavior of fused deposition modeling (FDM) manufactured surfaces and test the accuracy of existing mathematical models such as Amontons–Coulomb, Tabor–Bowden, and variations of Hertz Contact model against empirical data.

Design/methodology/approach – Conventional frictional models Amontons–Coulomb and Tabor–Bowden are developed for the parabolic surface topography of FDM surfaces using variations of Hertz contact models. Experiments are implemented to measure the friction between two flat FDM surfaces at different speeds, normal forces, and surface configuration, including the relative direction of printing stripes and sliding direction and the surface area. The global maximum measured force is considered as static friction, and the average of the local maxima during the stick-slip phase is assumed as kinematic friction. Spectral analysis has been used to inspect the relationship between the chaos of vertical wobbling versus sliding speed.

Findings – It is observed that the friction between the two FDM planes is linearly proportional to the normal force. However, in contrast to the viscous frictional model (i.e., Stribeck), the friction reduces asymptotically at higher speeds, which can be attributed to the transition from harmonic to normal chaotic vibrations. The phase shift is investigated through spectral analysis; dominant frequencies are presented at different pulling speeds, normal forces, and surface areas. It is hypothesized that higher speeds lead to smaller dwell-time, reducing creep and adhesive friction consequently. Furthermore, no monotonic relationship between surface area and friction force is observed.

Research limitations/implications – Due to the high number of experimental parameters, the research is implemented for a limited range of surface areas, which should be expanded in future research. Furthermore, the pulling position of the jaws is different from the sliding distance of the surfaces due to the compliance involved in the contact and the pulling cable. This issue could be alleviated using a non-contact position measurement method such as LASER or image processing. Another major issue of the experiments is the planar orientation of the pulling object with respect to the sliding direction and occasional swinging in the tangential plane.

Practical implications – Given the results of this study, one can predict the frictional behavior of FDM manufactured surfaces at different normal forces, sliding speeds, and surface configurations. This will help to have better predictive and model-based control algorithms for fully AM manufactured mechanisms and optimization of the assembly manufactured systems. By adjusting the clearances and printing direction, one can reduce or moderate the frictional forces to minimize stick-slip or optimize energy efficiency in FDM manufactured joints. Knowing the harmonic to chaotic phase shift at higher sliding speeds, one can apply certain speed control algorithms to sustain optimal mechanical performance.

Originality/value – In this study, theoretical tribological models are developed for the specific topography of the FDM manufactured surfaces. Experiments have been implemented for an extensive range of boundary conditions, including normal force, sliding speed, and contact configuration. Frictional behavior between flat square FDM surfaces is studied and measured using a Zwick tensile machine. Spectral analysis, auto-correlation, and other methods have been developed to study the oscillations during the stick-slip phase, finding local maxima (kinematic friction)

The authors would like to thank P.J. van Swaaij (Andries) from the Chair of Elastomer Engineering and Technology at University of Twente, for his kind support. The study is funded by Technological Pioneering in HealthCare (PIHC) voucher “PneuARMM: pneumatically actuated robot for minimally invasive MRI guided interventions” a collaboration of University of Twente (UT), Medisch Spectrum Twente (MST) and PneuRobotics™. This work was also supported in part by the European Research Council (ERC) under Grant #638428 (Project ROBOTAR).

Received 21 June 2019
Revised 21 February 2020
Accepted 23 March 2020

The current issue and full text archive of this journal is available on Emerald Insight at: <https://www.emerald.com/insight/1355-2546.htm>



Rapid Prototyping Journal
26/6 (2020) 1095–1102
© Emerald Publishing Limited [ISSN 1355-2546]
[DOI 10.1108/RPJ-06-2019-0171]

and dominant periodicity of the friction force versus sliding distance. Precise static and kinematic frictional coefficients are provided for different contact configurations and sliding directions.

Keywords Friction, Tribology, Fused deposition modeling (FDM), 3D printing, Additive manufacturing (AM)

Paper type Research paper

1. Introduction

Additive manufacturing (AM) technology [also known as 3D printing (ASTM-F2792-12, 2012)] enables developers to design parts with higher topological and geometric complexities. Some concave or hollow geometries are not feasible by conventional machining, hereafter referred to as subtractive manufacturing (SM). AM entails lower costs and lead-time for low-volume and customized production. Being a direct digital manufacturing method, AM also offers a faster research and development process for innovative industries (Chua *et al.*, 2010). Non-assembly production is also one of the unique features of AM where a complete integrated functional mechanism, with embedded moving joints, can be printed without the need for further assembly (also known as assembly printing). Currently, AM is experiencing a major transformation from demonstrative/rapid prototyping to functional manufacturing, where the parts are being directly used as/ in the actual products (Farimani and Misra, 2018; Farimani *et al.*, 2020). Therefore, the final properties of the printed parts, including geometric, mechanical, tribological, electromagnetic and thermal characteristics, should be better understood. Medical, food, space and do-it-yourself industries are some of the application areas where the AM technology is already deployed, or significant development is undergoing (Govender *et al.*, 2020; Attaran, 2017; Fox, 2020).

A wide variety of AM methods are available, with various price choices for hobbyists and professionals. Fused deposition modeling (FDMTM), also known as material extrusion (ASTM-F2792-12, 2012), is one of the most popular commercially available AM methods. FDM machines deposit stripes of melted thermoplastics such as acrylonitrile butadiene styrene (ABS) and polylactic acid (PLA), to form a 3D object. In comparison to other AM methods, FDM parts are affordable and have good mechanical performance. Particularly, FDM-ABS parts have the advantage of being environmentally friendly, thanks to the recyclability of the material. Besides, they present other properties, such as being chemically inert and self-lubricating. These make FDM-ABS ideal for tribological applications and manufacturing of disposable parts, for example in surgical applications (Farimani and Misra, 2018; Farimani *et al.*, 2020).

One of the primary drawbacks of AM parts in comparison to SM is the fact that they bear rougher surface topographies and nonuniformly distorted geometries (Luis Pérez, 2002; Nourghassemi, 2011; Taufik and Jain, 2016; Alsoufi and Elsayed, 2017). This complicates the manufacturing of airtight fluidic systems (i.e., hydraulic and pneumatic), as well as precise mechanisms with moving joints (e.g. robotics). Friction not only reduces the controllability and accuracy/precision of the mechanical systems but also adversely affects their energy efficiency. Understanding the frictional behavior of the AM surfaces is a crucial step toward production and controlling of fully 3D printed mechanisms (e.g. assembly printing).

The dry friction phenomena can present chaotic behavior, and without experiments, it is challenging to estimate it in a specific

system (Briscoe and Sinha, 2002; Myshkin *et al.*, 2005; Rymuza, 2007; Unal and Mimaroglu, 2012; ASTM-D1984-14, 2014). A plethora of research has been done on the friction of polymers, and different frictional coefficients have been reported: for steel on ABS with presumably smooth surfaces static 0.35 and dynamic 0.30 (Totten, 2017), static 0.2 and dynamic 0.15 (Ellis and Smith, 2008), average dynamic 0.376 (Bashford, 1996). Difallah *et al.* reported the effects of additives on mechanical and wear properties of ABS (Ben Difallah *et al.*, 2012). Leacock *et al.* (2014) studied the effect of sliding distance on frictional coefficients between FDM printed ABS surface and smooth titanium using the strip-pull-friction-test, at different normal pressures (2.36–7.08) MPa, speeds (50–250) mm/min and sliding directions (perpendicular to stripes and 45°). They showed that the friction increases by sliding distance, reaching a maximum when ripples of the surface are worn out. Gurralla *et al.* investigated the effect of load and sliding speed on pin-on-disk friction of FDM-ABS parts, observing an increase of friction by wear (Gurralla and Regalla, 2014). Dawoud *et al.* (2015) explored the effects of 3D printing parameters such as gap and scaffolding angle on wear. Boparai *et al.* investigated the effects of load and wear on friction in a pin-on-disk apparatus (Singh Boparai *et al.*, 2016). Perepelkina *et al.* (2017) studied the effect of filling factor, temperature and wear on the friction of FDM printer tribopairs. Beg *et al.* (2017) studied the abrasive properties of FDM-ABS parts. Farstad *et al.* (2017) investigated the friction of printed thermoplastic elastomers on smooth surfaces. Sood *et al.* developed heuristic methods (i.e., artificial neural networks) to predict the effect of printing parameters on precision, accuracy and tribomechanical properties of AM parts (Sood *et al.*, 2010; Equbal *et al.*, 2010; Sood *et al.*, 2012).

Nevertheless, the tribological characteristics of 3D printed FDM-ABS surfaces are yet to be fully understood. Former studies are mere experimental, not considering the surface topography of the FDM parts. They have been mostly performed between FDM/ABS/Polymers and other materials. Therefore, the results are not necessarily extendable to the frictional behavior of fully 3D printed mechanisms. In this study, friction between two sets of identical flat surfaces made of FDM manufactured ABS using Stratasys[®] (Rehovot, Israel) Fortus[®] –250MC is explored. A Zwick[®] tensile machine (ZwickRoell, GA, USA) measures the pulling force against displacement, experimenting effects of normal force, printing direction, sliding direction, surface area and sliding speed on friction. Experiments for validation and parameter identification, follow mathematical modeling for surface topography and friction. Eventually, the theoretical models are validated against the empirical data.

2. Mathematical models

The friction force between two flat surfaces depends on various factors such as normal contact pressure, lubrication, dwell-time, sliding speed and surface topography. Different models have been developed for friction, prominently Coulomb-

Amontons (CA) model, which describes the friction force F_f between two dry surfaces with random roughness as linearly proportional to the normal force F_N :

$$F_f = \mu_f F_N, \quad (1)$$

where μ_f is the coefficient of friction (CoF). In [equation (1)], the μ_f is dimensionless if both F_N and F_f carry identical dimensions (N). Bowden *et al.* (1943) showed that the CA-CoF at high normal pressures [1], where surface asperities experience plastic deformation, is proportional to yield shear stress τ_y (MPa) divided by hardness H in Brinell scale (BHN), of the softer material:

$$\mu_f \approx \frac{\tau_y}{H}. \quad (2)$$

A yield shear stress of (30–45) MPa and a Brinell hardness of (95–100) MPa have been reported for ABS (Ellis and Smith, 2008; Bashford, 1996; STRATASYS, 2020; ASTM-D732-17, 2017), therefore an approximate CA-CoF of 0.3–0.45 is to be expected. Although the CA model is simple and practical, it does not represent the effects of surface topography, contact area and sliding speed.

2.1 Surface topography

The binomial Tabor–Bowden (TB) equation is one of the primary models describing the effects of surface topography, normal force and mechanical properties of the materials on friction (Bowden and Tabor, 1954; Yamaguchi, 1990; Tabor, 1974; Blau, 2008). The TB model divides the friction force into two distinct parts:

$$F_f = F_a + F_m, \quad (3)$$

where F_a and F_m are the adhesive and mechanical components, respectively. F_m is a collective term including several forces such as internal hysteresis of the materials due to the visco-elastic/plastic deformation (i.e., cohesion), as well as abrasion of the contact surfaces (also referred to as wear, grooving, scratching or plowing/ploughing in the literature). Practically plowing is considered negligible if the difference between the hardness of two surfaces is less than 20% (Van Beek, 2009). This applies to our case, considering that adjacent surfaces are identical. The adhesive force F_a (N) is mainly due to the intermolecular/chemical interactions between the two contacting surfaces. Adhesion has been described as:

$$F_a = \tau_s A_r, \quad (4)$$

where A_r (m^2) is the real contact area, and τ_s (Pa) is the shear adhesion strength. In the following sections, different models describing these two terms are elaborated:

2.1.1 Contact area

For rough surfaces, the actual contact area A_r is significantly smaller than the apparent surface area A_a . For perfectly random topographies, the ratio of real to apparent contact areas is linearly proportional to the normal force (Greenwood *et al.*, 1966). However, the real contact area for defined topographies should be calculated analytically, using variations of the Hertz contact model. It is known that parts made by FDM have a parabolic surface profile (Taufik and Jain, 2016; Alsoufi and Elsayed, 2017). As a

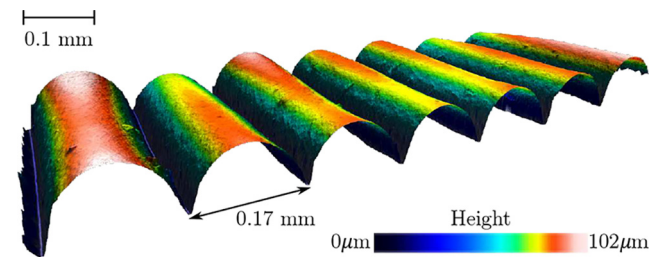
confirmation, (Figure 1) also shows a magnification of the surfaces made by a Fortus[®] –250MC 3D printer, using a Sensofar[®] (Barcelona, Spain) microscope (optical profilometer for non-contact 3D metrology). It can be seen that the 3D printed surface comprises parallel cylindrical stripes with diameters of 0.17 mm. The observation is in agreement with the minimum layering thickness used for printing, also reported for this particular 3D printer. The Stratasys[®] Insight[®] slicer has been used to generate the tool path. Default settings have been used as listed in the Table 1.

The Fortus[®] machine prints parts with stripes on the side walls horizontally aligned. The printer also fills internal cavities with stripes at 45° angle by default, leading to stripes on bottom surfaces with the same angle. Considering that printed parts have two different surfaces (top/bottom and side), various sliding scenarios exist (Figure 2).

For example, two side surfaces can have parallel (SS-Par) or perpendicular (SS-Per) alignments. When parallel, the relative motion can be alongside the cylinders' direction (SS-Par-Par) or perpendicular (SS-Par-Per). Therefore, there are three different possibilities for side-side (SS) configuration. In a parallel configuration, each cylinder can be either in contact with a single-cylinder from the opposite side (Par-Min) or with two (Par-Max) (Figure 2). Therefore, depending on the relative alignment of the cylinders, four different contact models (Par-Min, Par-Max, Perpendicular and Inclined) are considered.

The contacts between individual pairs of stripes can be calculated from variants of the Hertz model, if the deformations

Figure 1 Surface magnification of a 3D printed part made of ABSplus[®] -P430, using Stratasys[®] Fortus[®] -250MC

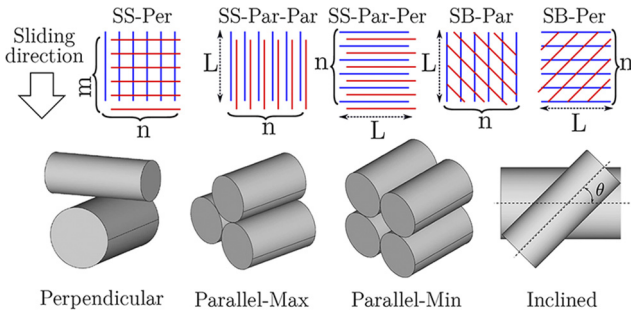


Notes: Sensofar[®] optical profilometer has been used to scan the surface topography. The measurement that the surface of the 3D printed parts comprises a series of parallel cylinders with a diameter of approximately 0.17 mm

Table 1 The default settings in Stratasys Insight slicer software

Part interior style	Sparse-high density
Visible surface style	Enhanced
Support style	SMART
Model material	ABS-P430
Support material	ABS-SR30
Slice height	0.1778 mm
Merge open curve tolerance	0.1270 mm
Curve filtering tolerance	0.0102 mm
Contour width	0.3556 mm
Enhanced visible rasters	0.3556 mm
Enhanced internal rasters	0.4572 mm

Figure 2 Different sliding scenarios considering the printing surface (bottom/top B and side S) and sliding directions (parallel Par and perpendicular Per) were experimented



Notes: Based on the alignment of the two surfaces, the printing stripes can be parallel (SS-Par), perpendicular (SS-Per), or inclined (SB) with an angle of $\theta = 45^\circ$. In SS-Par alignment two different contact scenarios should be considered where each cylinder is in contact with one (Parallel-Min) or two (Parallel-Max) cylinders from the adjacent surface

stay within the elastic range. Other assumptions of the Hertzian contact models are that the effect of adhesion on contact is negligible, and the diameter of the contact area compared to the diameter of the main objects is insignificant. For identical parallel cylinders (SS-Par) the Radzimovsky model (Radzimovsky, 1953; Young and Budynas, 2002; Pereira et al., 2011; Skrinjar et al., 2018), describes the width of contact a_c (m) as:

$$a_c = 2.15 \sqrt{\frac{F_N^* R}{LE}}, \quad (5)$$

where F_N^* (N) is the total contact force across one pair of cylinders with a radius of R (m), and E (Pa) is the elastic modulus, and L (m) is the length of the contact alongside the cylinder's axis. For the special case of identical perpendicular cylinders, the contact can be considered circular, calculated from the contact between a plane and a sphere of the same radius (Johnson, 1985; Flores and Lankarani, 2016). From the Hertz–Goldsmith model, the radius r_c (m) of circular contact between a sphere and a plane of the same material is:

$$r_c = \left(\frac{3F_N^* R}{4E} \right)^{\frac{1}{3}}. \quad (6)$$

For inclined cylinders, the contact area is elliptic (Puttock and Thwaite, 1969; Williams and Dwyer-Joyce, 2001). However, for simplicity in the case of identical cylinders with an angle of $\theta = 45^\circ$, it can be approximated with the circular contact between a plane and a sphere with an average radius of $R_c \approx \sqrt{2}R$. For parallel alignments, the total real and apparent contact areas can be calculated from the geometry of the cases:

$$\text{Min} : \begin{cases} A_r = na_c L \\ A_a = 2nRL \end{cases}, \quad \text{Max} : \begin{cases} A_r = 2na_c L \\ A_a = 2nRL \end{cases} \quad (7)$$

where n is the number of rows and L is length of the cylinders. In perpendicular configuration the contact areas are:

$$\begin{cases} A_r = nm\pi r_c^2 \\ A_a = nm4R^2 \end{cases}, \quad (8)$$

where nm is the number of rows \times columns, including all contact points. For inclined configuration the approximate number of contacts can be calculated from:

$$n_e \approx \frac{nL \sin \theta}{2R}, \quad (9)$$

and contact areas can be calculated consequently as:

$$\begin{cases} A_r \approx n_e \pi r_c^2 \\ A_a = 2nRL \end{cases}. \quad (10)$$

Considering that equations (5) and (6) represent individual contacts, extending them to the whole contact surface and combining them with equations (7), (8) and (10) yields:

$$A_r = k_1 \sqrt{\frac{F_N}{E}} A_a^{\frac{1}{2}}, \quad (11)$$

for parallel alignments, where $k_1 = 3.04$ for Min and $k_1 = 2.31$ for Max contact scenarios, and:

$$A_r = k_2 \left(\frac{F_N}{E} \right)^{\frac{2}{3}} A_a^{\frac{1}{3}}, \quad (12)$$

for perpendicular ($k_2 = 1.63$) and for inclined ($k_2 = 1.83$) surface configurations. In above equations F_N is the total normal force between the two surfaces, which is distributed uniformly across the contact area. Also, the k_s coefficients are dimensionless.

2.1.2 Adhesion

Amuzu et al. (1977) have shown that the adhesion shear strength in polymers is close to their bulk shear strength. Hence, an adhesive shear strength τ_s in the same order as (15–27) MPa for ABS is to be expected. However, to account for the effect of contact pressure, a linear relationship has been proposed by Bowden et al.:

$$\tau_s = \tau_0 + \alpha P_m, \quad (13)$$

where $P_m = F_N/A_r$ (Pa) is the mean effective contact stress and α is the dimensionless piezo coefficient of adhesion (Bowden and Tabor, 1954). Integrating equations (13), (3) and (4) yields:

$$F_f = \tau_0 A_r + \alpha F_N, \quad (14)$$

and replacing A_r from equations (11) and (12) will describe the friction force versus normal force and apparent contact area for different surface configurations according to the TB model.

2.2 Sliding speed

A combination of different underlying phenomena determines dynamic friction in the system, including viscosity, creep and morphological vibrations. The self-lubricating characteristics of polymers can manifest itself as viscosity at certain conditions, wherein the presence of liquid film the Stribeck model could be used (Armstrong-Helouvry, 2012, 1990; Hess and Soom, 1990; Bo and Pavelescu, 1982). Sliding speed also affects

friction through vertical vibrations during the stick-slip effect. For instance, Al-Bender *et al.* extended the Tomlinson model to macro-scale periodical surfaces (Al-Bender *et al.*, 2004; Tomlinson, 1929). Furthermore, sliding speed can also affect the dwell-time (relaxation), consequentially altering friction. Kato *et al.* (1972) have described the effect of dwell-time on friction, showing that at a low sliding speed, more adhesive bonds are developed between the asperities of the contacting surfaces, increasing adhesive force. The actual contact area increases by time due to creep, decreasing the coefficient of friction at higher speeds (Rabinowicz, 1995).

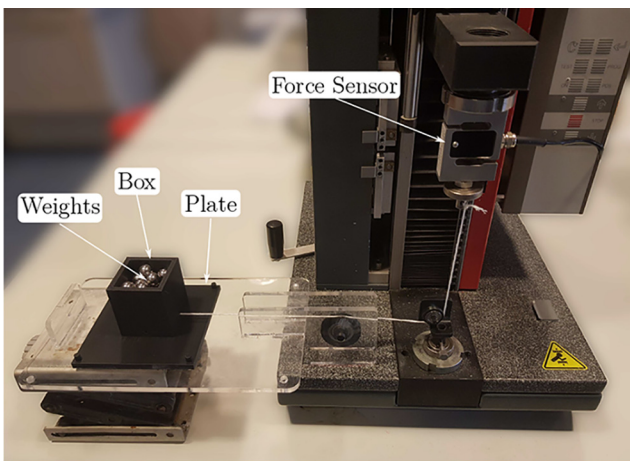
3. Experiments

To investigate the validity of the developed mathematical models a series of experiments are implemented. Frictional behavior between two 3D printed parts (a box and a plate) is studied (Figure 3). Different contact configurations are considered including the effects of surface area, printing direction (top/bottom and side) and sliding directions with regards to the printed strips (parallel, perpendicular and inclined).

As shown in (Figure 3), a Zwick® tensile machine is used to pull the box on top of the plate, and to measure the sliding force versus jaw displacement. Experiments are repeated for different pulling speeds (5-1800) mm/min, normal forces (40-250) g, different surface configurations (bottom/side-parallel/perpendicular) and surface areas $A_a = (900-2500)$ mm². Raw measurement data can be found at the provided repository (GitHub, 2020).

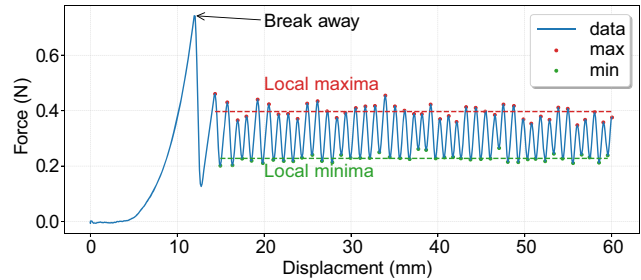
Figure 4 shows a sample measurement for a surface area of 0.0025 m², normal force of 232 g and pulling speed of 300 mm/min. It can be seen that when the pulling process starts, first the measured force rises, while energy is being stored in the

Figure 3 A Zwick® tensile machine is used to measure friction force between the two 3D printed surfaces



Notes: A flat square surface with a side length of 10 cm is fixed to the ground while a box, with different surface areas, is being pulled on top of it. The normal force between the two surfaces is controlled by changing the weights inside the box. Force sensor attached to the machine measures the force while the position is also being recorded simultaneously

Figure 4 Force versus displacement (of the force-cell) measurements by the Zwick® tensile machine, for a normal force of 232 g, a pulling speed of 300 mm/min, a square apparent surface area of 0.0025 m², between the bottom surface and side surface, with rows parallel to the direction of sliding (BS-Par)



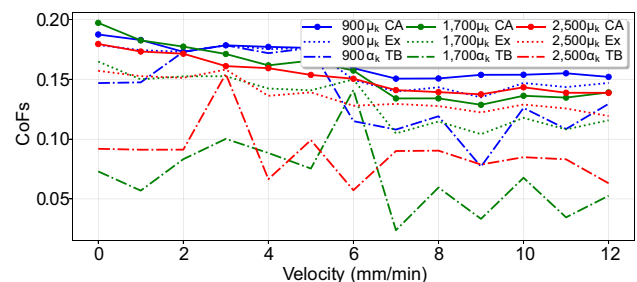
adhesive bonds of the contact surfaces, as well as the cable. At some point the intermolecular conjunctions between the contact surfaces collapse and a phase shift from static to kinetic friction happens. Stick-slip effect in the kinetic phase causes an oscillatory force measurement.

Measured data are analyzed to find the maximum global force (i.e., break away static friction) in addition to the average of local maxima (representing kinetic friction), average local minima and periodicity of the oscillations during the kinetic phase. Three different spectral analysis methods are developed to calculate the periodicity and local extremes, including Fourier transform, autocorrelation and manual filtering (GitHub, 2020).

4. Analysis

As expected, it is observed that normal force is the dominant influencing factor in both static and kinetic friction forces. However, attempts to fit the TB models lead to incoherent coefficients at different pulling speeds (Figure 5). It can be seen that surface area has a noticeable but non-monotonic effect on friction force. One interpretation could be that the Hertz models are not representative of these surfaces' contact behavior. An

Figure 5 Coefficients of kinematic friction μ_k for the CA and Ex models, and piezo coefficient of adhesion α_k from the TB model for SS-Per surface configuration at different pulling speeds (5-1800) mm/min and apparent surface areas $A_a = (900-2500)$ mm²



Note: It can be seen that the TB model leads to incoherent results at different speeds and the effect of apparent surface area is noticeable but non-monotonic

extended CA model with an offset (F_0) representing an initial surface adhesion, appears to be the most reliable representation of the measurements:

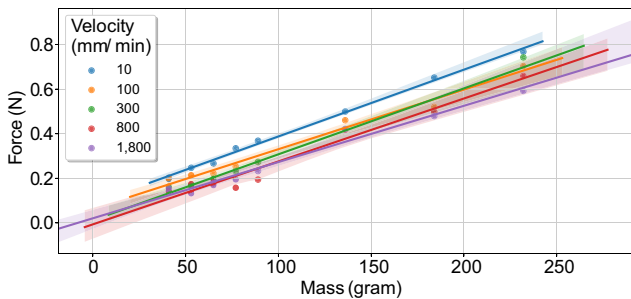
$$F_f = \mu F_N + F_0 \tag{15}$$

Figure 6 demonstrates the linearity of the correlation between friction-normal forces, including linear interpolations and error bands at different sliding speeds. The average static and kinetic friction coefficients in general are calculated (Table 2).

Surface configurations (alignment and sliding direction) are shown to be the second influencing parameter. SS-Par-Per configuration shows the highest friction forces followed by SS-Par-Par and SS-Per. The fact that SS-Par-Per presents higher friction forces than SS-ParPar, while SS-Par-Per has a smaller contact area, can be attributed to the formerly neglected deformation factor F_m from the TB model.

In contrast to viscous model, at higher speeds an asymptotic decline in static and kinetic friction forces is observed. For example, Figure 7 shows average kinetic friction forces for different masses versus speed for BS-Par configuration with a 0.0025 m^2 surface area. This behavior can be assigned to the vertical wobbling and dwell-time reduction as previously mentioned. Similar behaviors have been reported for textured surfaces (Schneider et al., 2017, 2018). Figure 8 shows the dominant frequency of the slip-stick phase for the previous model at different speeds and normal forces. It was also observed that the oscillatory motion becomes less harmonic at pulling speeds higher than 200 mm/min while spending more time sliding during each oscillation. Therefore, it can decrease dwell-time significantly.

Figure 6 Static friction force versus normal force at different speeds for the measurements of Figure 5

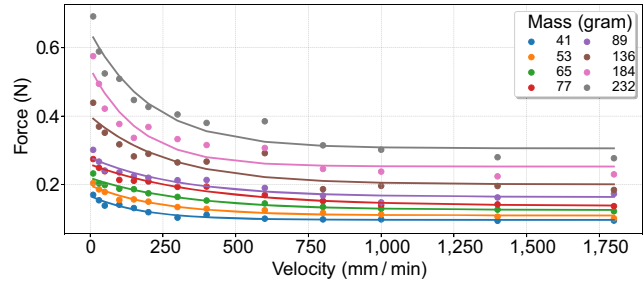


Note: The extended CA friction model with an initial adhesive force F_0 describes the linear relationship between the friction and normal force

Table 2 The average static and kinetic friction coefficients

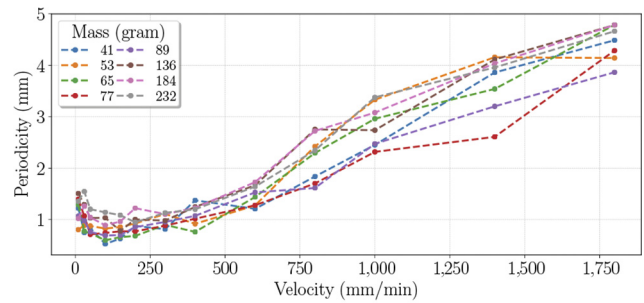
	μ_s	F_{0_s} (N)	μ_k	F_{0_k} (N)
SS-Par-Per	0.291	0.089	0.184	0.063
SS-Par-Par	0.245	0.073	0.157	0.048
SS-Per	0.220	0.048	0.143	0.026
Average	0.253	0.072	0.158	0.047

Figure 7 Average of maximum friction forces during the kinetic phase versus speed in addition to the interpolated graphs



Note: Kinetic friction force decreases at higher pulling speeds asymptotically reaching a minimum friction force

Figure 8 Average periodicity (dominant frequency of the oscillation during the kinetic phase) versus pulling speed for different normal forces



Note: The average dominant frequency slightly decreases from 0 to 200mm/min and then the oscillatory motion becomes less harmonic

5. Conclusion

In this study the frictional behavior of surfaces made by Stratasys® Fortus® –250mc FDM printer was studied. Effects of normal force, pulling speed, surface configuration and contact area on static and kinetic friction were investigated. Mathematical models were developed and compared against empirical data. Results reiterated the chaotic nature of friction phenomenon, showing it reflects drastically toward changes in the initial and boundary conditions. Some major assumptions of our model are the simplified geometrical shapes, linear elastic behavior, small contact area compared to the radius (Hertzian assumption), no adhesion or other surface forces (Hertzian assumption).

It was shown that the combination of the Hertz contact model and the TB frictional model does not represent the effect of surface topography and normal force on static and kinematic friction forces. A modified CA model with an initial force, representing the adhesive effect between the surfaces, appears to be the most coherent description. It is also demonstrated that the pulling speed has a significant effect on reduction of friction force, in contrast to the viscous model. Spectral analyses of the kinetic oscillations revealed a chaotic phase shift at certain pulling speeds. This can be described by vertical micro-vibrations affecting the dwell-time and therefore decrease the

adhesion between the surfaces. Further research including a wider range of normal force and surface areas is required to investigate the validity of this observation. It is suggested that the FDM manufactured surfaces should be considered among textured surfaces, as conventional friction models such as TB and Stribeck do not represent their frictional behavior.

Note

1 A tensile strength of 37 MPa has been reported for ABSplus®-P430 by Stratasys® (STRATASYS, 2020).

References

- Al-Bender, F., Lampaert, V. and Swevers, J. (2004), “Modeling of dry sliding friction dynamics: from heuristic models to physically motivated models and back”, *Chaos: An Interdisciplinary Journal of Nonlinear Science*, Vol. 14 No. 2, pp. 446-460.
- Alsoufi, M.S. and Elsayed, A.E. (2017), “How surface roughness performance of printed parts manufactured by desktop fdm 3d printer with pla+ is influenced by measuring direction”, *American Journal of Mechanical Engineering*, Vol. 5 No. 5, pp. 211-222.
- Amuzu, J.K.A., Briscoe, B.J. and Tabor, D. (1977), “Friction and shear strength of polymers”, *A S L E Transactions*, Vol. 20 No. 4, pp. 354-358.
- Armstrong-Helouvry, B. (1990), “Stick-slip arising from stribeck friction”, *Proceedings., IEEE International Conference on Robotics and Automation*, Vol. 2, pp. 1377-1382.
- Armstrong-Helouvry, B. (2012), *Control of Machines with Friction*, Vol. 128, Springer Science & Business Media.
- ASTM-D1984-14 (2014), Standard Test Method for Static and Kinetic Coefficients of Friction of Plastic Film and Sheeting, Standard, ASTM International, West Conshohocken, PA.
- ASTM-D732-17 (2017), “Standard test method for shear strength of plastics by punch tool”, *Standard*, ASTM International, West Conshohocken, PA.
- ASTM-F2792-12 (2012), Standard Terminology for Additive Manufacturing Technologies, Standard, ASTM International, West Conshohocken, PA.
- Attaran, M. (2017), “The rise of 3-d printing: the advantages of additive manufacturing over traditional manufacturing”, *Business Horizons*, Vol. 60 No. 5, pp. 677-688.
- Bashford, D. (Ed.) (1996), *Thermoplastics: Directory and Databook*, 1st ed., Chapman & Hall.
- Beg, M.S., Khan, M.D. and Khan, A.A. (2017), “Investigation on tribological behavior of fdm printed abs polymer”, *International Journal of Technical Research and Applications*, Vol. 5, pp. 75-77.
- Ben Difallah, B., Kharrat, M., Dammak, M. and Monteil, G. (2012), “Mechanical and tribological response of abs polymer matrix filled with graphite powder”, *Materials & Design*, Vol. 34, pp. 782-787.
- Blau, P.J. (2008), *Friction Science and Technology from CONCEPTS to APPLICATIONS*, CRC press.
- Bo, L.C. and Pavelescu, D. (1982), “The friction-speed relation and its influence on the critical velocity of stick-slip motion”, *Wear*, Vol. 82 No. 3, pp. 277-289.
- Bowden, F.P. and Tabor, D. (1954), *The Friction and Lubrication of Solids*, Oxford.
- Bowden, F.P., Moore, A.J.W. and Tabor, D. (1943), “The ploughing and adhesion of sliding metals”, *Journal of Applied Physics*, Vol. 14 No. 2, pp. 80-91.
- Briscoe, B.J. and Sinha, S.K. (2002), “Wear of polymers”, *Proceedings of the Institution of Mechanical Engineers, Part J: Journal of Engineering Tribology*, Vol. 216 No. 6, pp. 401-413.
- Chua, C.K., Leong, K.F. and Lim, C.S. (2010), *Rapid Prototyping: Principles and Applications*, 3rd ed., World Scientific.
- Dawoud, M., Taha, I. and Ebeid, S.J. (2015), “Effect of processing parameters and graphite content on the tribological behaviour of 3d printed acrylonitrile butadiene styrene”, *Materialwissenschaft Und Werkstofftechnik*, Vol. 46 No. 12, pp. 1185-1195.
- Ellis, B. and Smith, R. (Ed.) (2008), *Polymers: A Property Database*, 2nd ed., CRC Press.
- Eqbal, A., Sood, A.K., Toppo, V., Ohdar, R.K. and Mahapatra, S.S. (2010), “Prediction and analysis of sliding wear performance of fused deposition modelling-processed abs plastic parts”, *Proceedings of the Institution of Mechanical Engineers, Part J: Journal of Engineering Tribology*, Vol. 224 No. 12, pp. 1261-1271.
- Farimani, F.S. and Misra, S. (2018), “Introducing PneuAct: parametrically-designed MRI-Compatible pneumatic stepper actuator”, *Proceedings of IEEE International Conference on Robotics and Automation (ICRA)*, Brisbane, pp. 200-205.
- Farimani, F.S., Mojarradi, M., Hekman, E. and Misra, S. (2020), “PneuAct-II: hybrid manufactured electromagnetically stealth pneumatic stepper actuator”, *IEEE Robotics and automation letters*, available at: <http://bit.ly/2kr1rf3>
- Farstad, J.M.G., Netland, Ø. and Welo, T. (2017), “Surface friction of rapidly prototyped wheels from 3d-printed thermoplastic elastomers: an experimental study”, *Procedia Cirp*, Vol. 60, pp. 247-252.
- Flores, P. and Lankarani, H.M. (2016), *Contact Force Models for Multibody Dynamics*, Vol. 226, Springer.
- Fox, S. (2020), “Paradigm shift: do-it-yourself (DIY) invention and production of physical goods for use or sale”.
- GitHub (2020), “GitHub repository for experimental measurements and analytical codes”, available at: <http://bit.ly/2SloTYc>
- Govender, R., Abrahamsen-Alami, S., Larsson, A. and Folestad, S. (2020), “Therapy for the individual: towards patient integration into the manufacturing and provision of pharmaceuticals”, *European Journal of Pharmaceutics and Biopharmaceutics*, Vol. 149, pp. 58-76, doi: [10.1016/j.ejpb.2020.01.001](https://doi.org/10.1016/j.ejpb.2020.01.001)
- Greenwood, J.A., Williamson, J.B.P. and Bowden, F.P. (1966), “Contact of nominally flat surfaces”, *Proceedings of the Royal Society of London. Series A. Mathematical and Physical Sciences*, Vol. 295 No. 1442, pp. 300-319.
- Gurralla, P.K. and Regalla, S.P. (2014), “Friction and wear behavior of abs polymer parts made by fused deposition

- modeling (FDM)", *International Conference on Advances of Tribology*.
- Hess, D.P. and Soom, A. (1990), "Friction at a lubricated line contact operating at oscillating sliding velocities", *Journal of Tribology*, Vol. 112 No. 1, pp. 147-152.
- Johnson, K.L. (1985), *Contact Mechanics*, Cambridge University Press.
- Kato, S., Sato, N. and Matsubayashi, T. (1972), "Some considerations on characteristics of static friction of machine tool slideway", *Journal of Lubrication Technology*, Vol. 94 No. 3, pp. 234-247.
- Leacock, A.G., Cowan, G., Cosby, M., Volk, G., McCracken, D. and Brown, D. (2014), "Structural and frictional performance of fused deposition modelled acrylonitrile butadiene styrene (p430) with a view to use as rapid tooling material in sheet metal forming", *Key Engineering Materials*, Vol. 639, pp. 325-332.
- Luis Pérez, C.J. (2002), "Analysis of the surface roughness and dimensional accuracy capability of fused deposition modelling processes", *International Journal of Production Research*, Vol. 40 No. 12, pp. 2865-2881.
- Myshkin, N.K., Petrokovets, M.I. and Kovalev, A.V. (2005), "Tribology of polymers: adhesion, friction, wear, and mass-transfer", *Tribology International*, Vol. 38 Nos 11/12, pp. 910-921.
- Nourghassemi, B. (2011), "Surface roughness estimation for FDM systems", PhD thesis, Ryerson University, Toronto, ON.
- Pereira, C.M., Ramalho, A.L. and Ambrósio, J.A. (2011), "A critical overview of internal and external cylinder contact force models", *Nonlinear Dynamics*, Vol. 63 No. 4, pp. 681-697.
- Perepelkina, S., Kovalenko, P., Pechenko, R. and Makhmudova, K. (2017), "Investigation of friction coefficient of various polymers used in rapid prototyping technologies with different settings of 3d printing", *Tribology in Industry*, Vol. 39 No. 4.
- Puttock, M.J. and Thwaite, E.G. (1969), *Elastic Compression of Spheres and Cylinders at Point and Line Contact*, Commonwealth Scientific and Industrial Research Organization Melbourne.
- Rabinowicz, E. (1995), *Friction and Wear of Materials*, John Wiley & Sons.
- Radzimovsky, E.I. (1953), Stress distribution and strength condition of two rolling cylinders pressed together, Technical report, University of Illinois at Urbana Champaign, College of Engineering, Engineering Experiment Station.
- Rymuza, Z. (2007), "Tribology of polymers", *Archives of Civil and Mechanical Engineering*, Vol. 7 No. 4, pp. 177-184.
- Schneider, J., Braun, D. and Greiner, C. (2017), "Laser textured surfaces for mixed lubrication: influence of aspect ratio, textured area and dimple arrangement", *Lubricants*, Vol. 5 No. 3.
- Schneider, J., Djamiykov, V. and Greiner, C. (2018), "Friction reduction through biologically inspired scale-like laser surface textures", *Beilstein Journal of Nanotechnology*, Vol. 9 No. 1, pp. 2561-2572.
- Singh Boparai, K., Singh, R. and Singh, H. (2016), "Wear behavior of fdm parts fabricated by composite material feed stock filament", *Rapid Prototyping Journal*, Vol. 22 No. 2, pp. 350-357.
- Skrinjar, L., Slavič, J. and Boltežar, M. (2018), "A review of continuous contact-force models in multibody dynamics", *International Journal of Mechanical Sciences*, Vol. 145, pp. 171-187.
- Sood, A.K., Ohdar, R.K. and Mahapatra, S.S. (2010), "Parametric appraisal of fused deposition modelling process using the grey Taguchi method", *Proceedings of the Institution of Mechanical Engineers, Part B: Journal of Engineering Manufacture*, Vol. 224 No. 1, pp. 135-145.
- Sood, A.K., Equbal, A., Toppo, V., Ohdar, R.K. and Mahapatra, S.S. (2012), "An investigation on sliding wear of fdm built parts", *CIRP Journal of Manufacturing Science and Technology*, Vol. 5 No. 1, pp. 48-54.
- STRATASYS (2020), ABSPlus-P430 for Fortus 3D Production Systems.
- Tabor, D. (1974), *Friction, Adhesion and Boundary Lubrication of Polymers*, Springer US, Boston, MA, pp. 5-30.
- Taufik, M. and Jain, P.K. (2016), "A study of build edge profile for prediction of surface roughness in fused deposition modeling", *Journal of Manufacturing Science and Engineering*, Vol. 138 No. 6, pp. 061002-061002-11.
- Tomlinson, G.A. B.Sc. (1929), "Cvi. a molecular theory of friction", *The London, Edinburgh, and Dublin Philosophical Magazine and Journal of Science*, Vol. 7 No. 46, pp. 905-939.
- Totten, G.E. (Ed.) (2017), *Volume 18: Friction, Lubrication, and Wear Technology*, ASM Handbook. Washington, DC.
- Unal, H. and Mimaroglu, A. (2012), "Friction and wear performance of polyamide 6 and graphite and wax polyamide 6 composites under dry sliding conditions", *Wear*, Vol. 289, pp. 132-137.
- Van Beek, A. (2009), *Advanced Engineering Design: lifetime Performance and Reliability*, TU Delft, Delft.
- Williams, J.A. and Dwyer-Joyce, R.S. (2001), "Contact between solid surfaces", *Modern Tribology Handbook*, Vol. 1, pp. 121-162.
- Yamaguchi, Y. (1990), *Tribology of Plastic Materials: their Characteristics and Applications to Sliding Components*, Vol. 16, Elsevier.
- Young, W.C. and Budynas, R.G. (2002), *Roark's Formulas for Stress and Strain*, Vol. 7, McGraw-Hill, New York, NY.

Corresponding author

Foad Sojoodi Farimani can be contacted at: f.s.farimani@utwente.nl

For instructions on how to order reprints of this article, please visit our website:

www.emeraldgroupublishing.com/licensing/reprints.htm

Or contact us for further details: permissions@emeraldinsight.com